Composite Structures 154 (2016) 309–318

Contents lists available at ScienceDirect

Composite Structures

journal homepage: www.elsevier.com/locate/compstruct

A computational micromechanics approach to evaluate elastic properties of composites with fiber-matrix interface damage

Néstor Darío Barulich [a,b], Luis Augusto Godoy [a,c,*], Patricia Mónica Dardati [b]

[a] Instituto de Estudios Avanzados en Ingeniería y Tecnología, IDIT UNC-CONICET, Ciudad Universitaria, Av. Vélez Sarsfield 1611, X5016GCA, Córdoba, Argentina
[b] Facultad Regional Córdoba, Universidad Tecnológica Nacional, Maestro M. López esq. Cruz Roja Argentina, X5016ZAA, Córdoba, Argentina
[c] Universidad Nacional de Córdoba, FCEFyN, Ciudad Universitaria, Avda. Vélez Sarsfield 1611, X5016GCA, Córdoba, Argentina

ARTICLE INFO

Article history:
Received 25 April 2016
Revised 24 July 2016
Accepted 25 July 2016
Available online 26 July 2016

Keywords:
Composite materials
Computational micro-mechanics
Debonding
Finite Element analysis
Hygro-thermal damage

ABSTRACT

Computational micro-mechanics is employed in this work to evaluate effects of fiber-matrix interface damage on the elastic properties of polymer matrix composites with continuous glass fibers. It is assumed that damage affects local zones along the fiber and a sector on the perimeter around the fiber. Elastic modulii are evaluated using Finite Element analysis, for a range of values in damage parameters considered. The occurrence of bi-modular behavior, with differences in Young's modulus under tension and compression, has been represented by contact without friction. Based on extensive parametric results, a Least Squares Method is employed to derive analytical expressions for each material property as a function of damage parameters. In most cases the elastic modulus has a nonlinear relation with the damage parameter in the length of the fiber, with the exception of the transverse elastic modulus under tension. The analytical expressions are used to couple micro and macro scales in an off-line scheme, without the need to perform in-time micro-scale computations.

1. Introduction

The analysis of fiber-reinforced composite materials has been traditionally performed using what is known as Classical Lamination Theory (CLT) (see for example Ref. [1]) or more refined higher order theories (such as in Ref. [2]), in which the heterogeneous fiber-matrix material is reduced to an equivalent homogeneous material for a lamina at the macro level. Thanks to increasing hardware and software capabilities, it is now possible to model this problem at the micro level to represent localized effects, such as defects and damage. However, to recover the complete picture it is necessary to couple the micro and macro levels, and this may be a costly procedure when both levels are modeled by means of Finite Elements in a non-linear analysis. This paper discusses an off-line procedure to couple the micro and macro levels, in which results of the micro level are previously computed.

The occurrence of damage at the fiber-matrix interface in glass fiber reinforced polymers (GFRP) has been identified for structures built in moisture and temperature environments. Evidence of such damage has been provided by laboratory testing [3] in which coupons were immersed in water at temperatures of 60–80 °C for several months, then were tested to evaluate their mechanical properties and damage was observed by scanning electron microscopy (SEM). The work reported by Kajorncheappunngam et al. [3] considered coupons at ambient and 60 °C temperatures in various water solutions for five months. These authors concluded that the elastic modulus in GFRP was not affected by hygro-thermal process, but significant reductions in strength were identified due to matrix cracking and fiber-matrix interface debonding. Interface damage was observed with the aid of SEM. In a study of resin and composite degradation in off-shore wind turbines, Faguaga et al. [4] found significant levels of matrix and interface degradation at 80 °C. For randomly oriented long fibers, some 20% reduction in modulus of elasticity was obtained, together with observations of fracture surfaces at the interface. For long, glass fibers in vinylester matrix, moisture absorption under short time exposure was studied by De la Osa et al. [5]. The influence of fiber orientation (either unidirectional, bidirectional, or randomly oriented) was investigated by means of bending tests on the material with hygro-thermal degradation.

Kotani et al. [6] tested a single fiber in matrix to measure consequences of hygro-thermal degradation in de-ionized water at 80 °C during 1000 h. The authors proposed a model and showed that there was a loss of strength arising from the degradation at

* Corresponding author at: Instituto de Estudios Avanzados en Ingeniería y Tecnología, IDIT UNC-CONICET, Córdoba, Argentina.
E-mail address: luis.godoy@unc.edu.ar (L.A. Godoy).

http://dx.doi.org/10.1016/j.compstruct.2016.07.065
0263-8223/

the fiber-matrix interface. The elastic modulus did not change, most likely because testing was performed in the direction of the fiber.

More advanced experimental techniques have also been employed to identify damage at the micro level: X-ray Computed Tomography (XCT) was used in Refs. [7,8] to carry out a 3D scanning of the microstructure in short-fiber and 3D textiles composites, respectively. The XCT technique captures details such as fiber length and orientation.

Observations and testing such as those described above are not sufficient to describe the actual mechanisms leading to damage. The mechanisms may be dominated by physical or chemical sources, but no attempt has been made to model that part of the problem. Instead, damage models start from the assumption that damage has already occurred at the micro-structural level, and interest focuses on the changes occurred with respect to the undamaged configuration. Damage models of this kind were reported by Kamiński [9] as semi-circular voids at the interface, in which the radius and number of voids were variables of the model. A similar approach was carried out by Godoy et al. [10] to identify stress redistributions caused by interface damage at Unit Cell (UC) level.

Teng [11] evaluated axial and longitudinal shear modulus (G_{12} and G_{13}) of a composite having symmetric arrangements of cracks at the top and bottom of a fiber. The damage parameter in this case is the angle of debonding between matrix and fiber, with angle values ranging from 0 to 2π. The results show that there is a loss of the initial transverse isotropy of the material. The shear modulus in the axial direction in a fiber reinforced composite having interface debonding has been investigated in Ref. [12] using a statistical distribution of damage size and taking into account that fibers may or may not have interface damage. It was found that the largest reductions in elastic shear modulus occur for a fiber volume fraction of 80%.

Kim et al. [13] investigated a configuration with interface cracks having random size and orientation to evaluate the transverse modulus of elasticity and transverse shear modulus. For a 30% fiber volume fraction, a reduction in modulii higher than 50% was reported. Studies performed by Kushch et al. [14] at a UC level including interface damage allowed evaluation of the elastic constitutive tensor at macroscopic level. The results were based on a previous work by the authors [15] for a periodic composite having open cracks, but contact between surfaces was not taken into account.

For a unidirectional composite with metal matrix the influence of complete debonding on the transverse elastic properties was studied in Ref. [16]. By means of simplified analytical expressions, the authors evaluated tensile and compressive modulus; such materials having different properties in tension and compression are referred to as bimodular or bimodulus materials in the literature. The transverse modulus, transverse shear modulus, and transverse Poisson's ratio were modeled by Shan and Chou [17] for composites by accounting for separation and contact at the interface.

Teng [18] represented complete detachment at the interface in a fiber-reinforced composite at a Representative Volume Element (RVE) including 100 fibers in a square configuration. The number of fibers having damage was increased until all fibers exhibited interface damage, and tensile and compressive Young's modulus and Poisson's ratio were obtained in terms of fiber volume fraction.

Another way to model interface damage is by means of a layer surrounding the fiber, with properties based on assumed load-transfer mechanisms between matrix and fiber. This model is capable of representing strong or weak interfaces [19–21]; as a limit case it can account for complete interface separation but cannot represent a bimodular behavior.

Current needs in modeling a pre-existing damage (without explicit reference to the source of damage) require using micro-level parameters, such as phase fractions, size and position of damage, to obtain macro-level properties. The models reviewed above have features that are not observed in tests, such as continuous damage in the direction of the fiber (in a 2D representation) versus damage being limited to a sector along the fiber (in a 3D representation).

This paper focuses on the computational modeling of micromechanics in GFRP materials having localized damage at the fiber-matrix interface. Through the use of a 3D model, the aim is not only to understand the influence of damage on macro properties, but also to derive the elastic macroscopic properties of an orthotropic unidirectional lamina by means of analytical functions written in terms of damage parameters at the micro level. Interest in such analytical formulation arises because these expressions can be easily incorporated at the macro level by means of CLT or in a Finite Element discretization of the structure by means of an off-line scheme, i.e. without the need to perform calculations at the micro-level during the solution of the structural problem at the macro-level.

2. Methodology

The domain at the micro-level is modeled in this work by means of computational micromechanics, CMM [22,23], in which two scales are considered: microstructural details are taken into account at a UC (a part of the heterogeneous material that includes the necessary information to represent the macroscopic behavior of interest); at the macro-level the material properties are assumed to be homogeneous with a mechanical behavior which is equivalent to the material modeled at the microscale. The analysis is performed by imposing strains to the UC in order to obtain the macroscopic variables that represent the material at the macro level by means of a post-process. Notice that XFEM, the Extended Finite Element Method, is also capable of solving this RVE problem including internal cracks [24].

Periodic Boundary Conditions (PBC) were used in this work to represent a periodic composite under finite strains. PBC have been described in the literature on computational micro-mechanics, such as in Refs. [25–27], among others.

Evaluation of elastic properties at macro-level requires that non-linearity of the contact problem should be taken into account, i.e. stresses and strains at the macro level are evaluated by taking into account crack opening and eventual load transfer caused by contact between crack surfaces. With stress and strain at the macro level, elastic properties can be obtained from them. For example, the elastic modulus E_2 in the direction 2 results in

$$E_2 = \frac{\sigma_{22}}{\varepsilon_{22}} \tag{1}$$

and the shear modulus G_{13} is

$$G_{13} = \frac{\sigma_{13}}{2\varepsilon_{13}} \tag{2}$$

Poisson's coefficients are next computed as

$$\nu_{ij} = -\frac{\varepsilon_{jj}}{\varepsilon_{ii}} \tag{3}$$

where ε_{ii} is the imposed strain, and ε_{jj} is the resulting strain (Eq. (4.32) in Ref. [1]).

At the UC, contact without friction was assumed to model interface cracking, and it was implemented using a penalty approach. The surface of an interface crack is divided into a master surface and a slave surface, which are associated to fiber and matrix, respectively. The model employed to represent the behavior in

direction normal to the contact surfaces (known as "hard contact") may be written as

$$\begin{aligned} &p = 0 \quad \text{for} \quad h < 0 \quad \text{(open), and} \\ &h = 0 \quad \text{for} \quad p > 0 \quad \text{(closed)} \end{aligned} \tag{4}$$

in which h (over-closure) is the penetration length of a slave node on the master surface, and p is the contact pressure associated to that node. Thus, contact between crack surfaces includes only normal compressive stresses between them.

The general purpose Finite Element program ABAQUS [28] was used in the unit cell computations, with quadratic, 15-node and 10-node elements identified as C3D15 and C3D10 in the ABAQUS nomenclature (see Fig. 1). Convergence studies were performed, reaching up to 82,000 elements and augmenting the penalty stiffness up to six orders of magnitude from the default value, which is 10 times the highest element stiffness in the model. Mesh densification was used at the ends of the damaged zones around the fibers; this, however, did not significantly change results (less than 0.1%) because a singularity in stress is limited to a small area and does not have a great impact on the stresses at the macro level.

To evaluate the quality of results obtained by the penalty technique, results were compared with those from a mixed formulation including Lagrange multipliers for specific UC with interface damage. In the mixed formulation the contribution of the contact constraint to the virtual work is given by

$$\delta\Pi = \delta p\, h + p\, \delta h \tag{5}$$

Considering small relative displacements between contact surfaces, the first variation of h becomes

$$\delta h = -\mathbf{n} \cdot (\delta \mathbf{u}_{N+1} - \delta \mathbf{x_0} - \xi_1 \delta \mathbf{v}_1 - \xi_2 \delta \mathbf{v}_2) \tag{6}$$

where $\mathbf{n}$ is the normal to the master surface; $\delta \mathbf{u}_{N+1}$ is the displacement variation of the slave node; $\delta \mathbf{x}_0$ is the variation of the position of the point on the master surface corresponding to the intersection of the normal that contains the slave point; ξ_1 and ξ_2 are used as parameters of the master contact surface; and the variations of the tangent vectors to the master surface are denoted by $\delta \mathbf{v}_1$ and $\delta \mathbf{v}_2$. Excellent agreement was obtained using both (penalty and mixed) implementations.

2.1. Geometry of unit cells

Two geometries were employed in this work to model the UC, as shown in Fig. 2: First a prismatic UC with a base given by a parallelogram of equal sides; second, a truncated octahedron. Both UC shapes were employed to model a composite with unidirectional fibers aligned in direction 1. Damage at the interface was included to be able to model problems such as hygro-thermal damage.

To model the microstructure in a periodic material it is possible to employ the concept of periodicity vectors (Oller et al. [29]). Three vectors of periodicity for each UC were used in this work; for the prismatic UC one has

$$\begin{aligned} \mathbf{P1} &= \beta Rf\, \mathbf{i} \\ \mathbf{P2} &= 2b\, \mathbf{j} \\ \mathbf{P3} &= 2b\, \cos(\theta)\mathbf{j} + 2b\, \sin(\theta)\mathbf{k} \end{aligned} \tag{7}$$

where Rf and lf are the fiber radius and length having an aspect ratio $\beta = lf/Rf$; θ and b are shown in Fig. 2b.

The value of b may be related to Vf, fiber volume fraction, as

$$b = Rf \sqrt{\frac{\pi}{4Vf\, \sin(\theta)}} \tag{8}$$

For the truncated octahedron domain, the periodicity vectors are

$$\begin{aligned} \mathbf{P1} &= lf\, \mathbf{i} \\ \mathbf{P2} &= \frac{lf}{3}\, \mathbf{i} + lf \sqrt{\frac{\mathbf{2}}{\mathbf{3}}}\mathbf{j} + \frac{\sqrt{\mathbf{2}}}{\mathbf{3}} lf\, \mathbf{k} \\ \mathbf{P3} &= \frac{\mathbf{2}}{\mathbf{3}} lf\, \mathbf{i} + \frac{\mathbf{2}\sqrt{\mathbf{2}}}{\mathbf{3}} lf\, \mathbf{k} \end{aligned} \tag{9}$$

in which the fiber length lf can be expressed as

$$lf = \sqrt{6}\, le \quad \text{with} \quad le = Rf \sqrt{\frac{\pi\sqrt{3}}{8\, Vf}} \tag{10}$$

le is the edge length of the truncated octahedron, as shown in Fig. 2a. The input data in this case is given by Rf and Vf.

For the prismatic domain, input data is given by Rf, Vf, β, and θ, from which values of lf and b are evaluated. Angle θ takes values of $\theta = 60°$ to obtain hexagonal (Hx) fiber configurations, or $\theta = 90°$ in square (Sq) configurations. In theory, upper boundaries to Vf are established when the fiber diameter is in contact with the UC boundary. For the prismatic UC domain, $Vf^{Max} = \pi/4 \cdot \sin(\theta)$ leading to $Vf^{Max} = 0.785$ for the Sq configuration, and $Vf^{Max} = 0.68$ for the Hx configuration.

For the truncated octahedron,

$$Vf^{Max} = \frac{3\sqrt{3}}{32}\pi = 0.51 \tag{11}$$

A hygro-thermal damage is represented in this work as a crack or separation at the fiber-matrix interface, and as such it always has a cylindrical shape. The location of damage is shown in Fig. 2, where the two planes of symmetry of the damage are

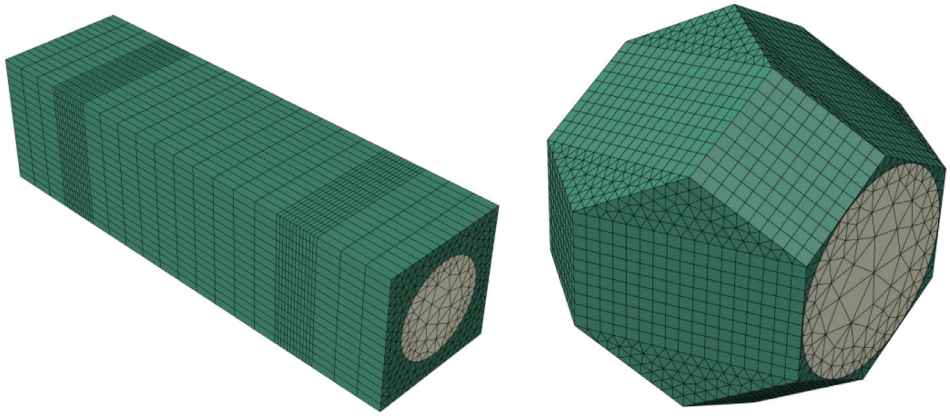

Fig. 1. Examples of Finite Element meshes: (a) Prismatic UC, (b) Truncated octahedron.

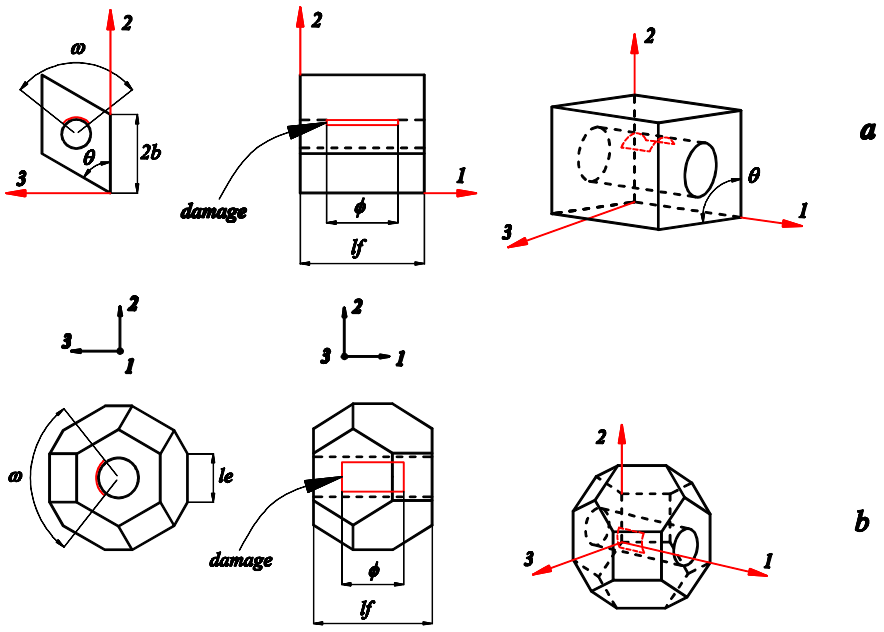

Fig. 2. Position and dimensions of damage in unit cells: (a) Prismatic; (b) Truncated octahedron.

parallel to planes identified as 1–2 and 2–3 for the prismatic UC, and to planes 2–3 and 1–3 in the octahedral UC. Two non-dimensional parameters are used to represent damage: *pd* is the damage parameter in the perimeter of the cross section of the fiber; and *ld* is the damage parameter along the length of the fiber. With reference to Fig. 2, both parameters can be evaluated as

$$ld = \frac{\phi}{lf}; \quad pd = \frac{\omega}{2\pi} \tag{12}$$

where ω is given in radians. Both, *ld* and *pd*, take values between 0 and 1, where 0 refers to an undamaged configuration, and 1 is for maximum damage level. Notice that for $\theta = 60°$, both types of UC represent the same fiber arrangement but are associated with different damage configurations, as shown in Fig. 3 for the same β value. To compare UC properties the orientation should be provided as shown in Fig. 3, so that damage in both cases is located in a similar way. Due to the position and orientation given to damage in both UC employed in this work, the properties along axis 2 in the prismatic UC are comparable to properties along axis 3 in the truncated octahedron.

2.2. Analytical form of numerical results

With the elastic properties given in terms of parameters *ld* and *pd*, Least Squares Method (LSM) was used to derive explicit relations between material elastic parameters and damage variables. Such analytical relations were subsequently used to model damage at the macro scale as pre-defined modified properties. The technique has been used for almost the same purpose by Kamiński [30].

Polynomial equations linear in the coefficients were used in all cases. In a few cases it was necessary to use nonlinear equations in the coefficients to obtain an improved representation. Equations were fitted by use of Levenberg-Marquardt method, as described in Ref. [31] (pp. 624–625).

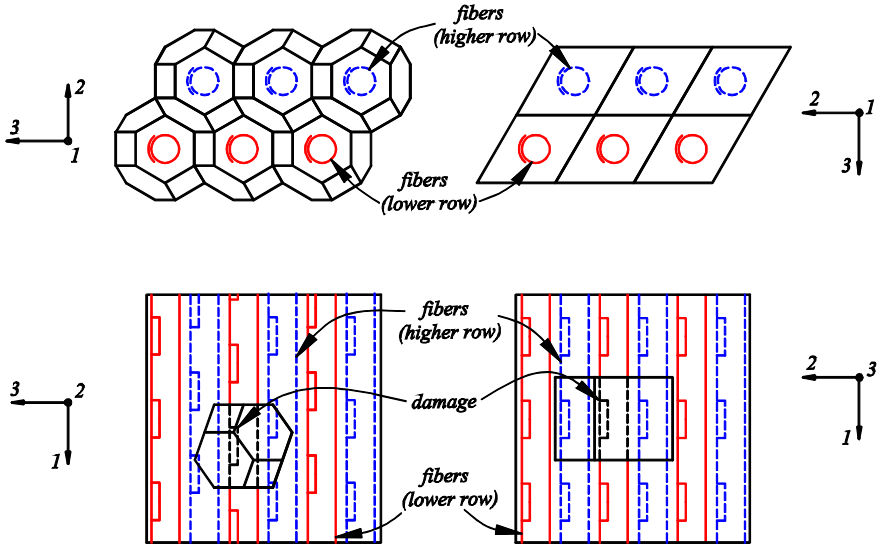

Fig. 3. Damage configurations considered in this work in unit cells.

3. Results

3.1. Validation for extreme cases

In a 2D model with interface damage, an assumption is made that damage affects the fiber in a continuous way in the direction of the fiber [18]; in a 3D model, this would be given by the condition $ld = 1$. Another extreme case occurs for $ld = 0$, in which the 2D model coincides with a 3D model without damage. Thus, 2D models may be seen as bounds to 3D models having more localized damage, as reflected by $0 \leqslant ld \leqslant 1$. These extreme cases are next used to confirm 3D models.

Specifically, a square fiber configuration (Sq) is assumed with $0 \leqslant pd \leqslant 1$ and Periodic Boundary Conditions. Because of space limitation, only the case $pd < 1$ is discussed next to compare results with values of elastic constants in the macro constitutive tensor with those given in Ref. [14].

Kushch et al. [14] considered fiber and matrix as linearly elastic and isotropic with $E_f = 107.848$ GPa, $\nu_f = 0.22$, $E_m = 6.453$ GPa y $\nu_m = 0.35$. The imposed strain is limited to a single tensile ε_{22} component. The constitutive equation at macro level is

$$\sigma_{ij} = C_{ijkl}\,\varepsilon_{kl} \tag{13}$$

Considering the imposed strain and the stress, yields

$$C_{2222} = \frac{\sigma_{22}}{\varepsilon_{22}} \tag{14}$$

Two-dimensional results are compared in Fig. 4 with those given in Ref. [14] for C_{2222}, showing excellent agreement.

2D and 3D models are next compared for a Sq arrangement using a prismatic UC with $\theta = 90°$, for various *Vf*, *ld*, and *pd* values. Values of $\beta = 5$, $E_f = 80$ GPa, $\nu_f = 0.2$, $E_m = 4$ GPa y $\nu_m = 0.35$ were assumed. Results for transverse shear modulus G_{23} are plotted in Figs. 5 and 6, whereas transverse elastic modulus in compression E_{3C} are given in Figs. 7 and 8. As *ld* approaches extreme values, it is seen that the 3D model tends to the 2D model.

3.2. Parametric studies

A specific composite having $E_f = 80$ GPa, $\nu_f = 0.2$, $E_m = 4$ GPa y $\nu_m = 0.35$ was considered, in which fiber and matrix were assumed as linearly elastic and isotropic. Fig. 9 shows the transverse elastic modulus E_{2T} with a Hx fiber configuration but having two different 3D damage distributions along the fibers. Such damage distributions were already shown in Fig. 3, for the prismatic and truncated octahedron UC geometries. Both UC have the same values of β, for $Vf = 50\%$.

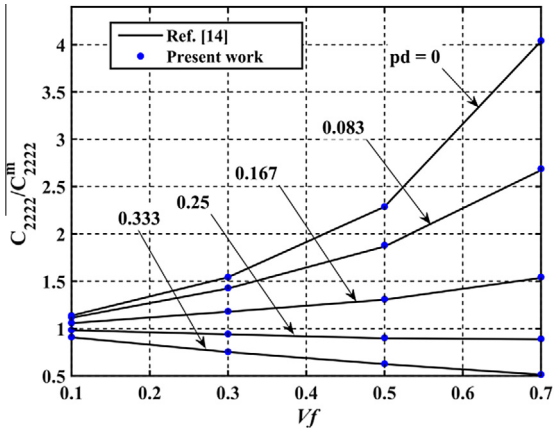

Fig. 4. Results for 2D model and Ref. [14] with Sq configuration and various values for the damage parameter *pd*.

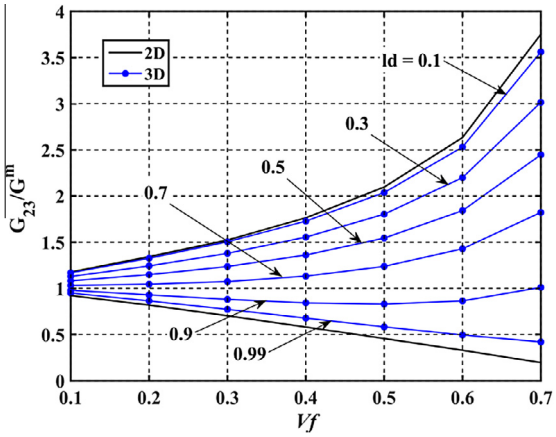

Fig. 5. Results for transverse shear modulus G_{23} for 3D model and 2D model with values of damage parameter $pd = 1$ and Sq configuration.

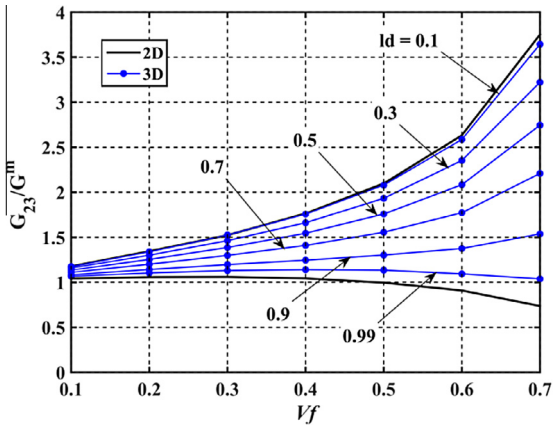

Fig. 6. Results for transverse shear modulus G_{23} for 3D model and 2D model with values of damage parameter $pd = 0.5$ and Sq configuration.

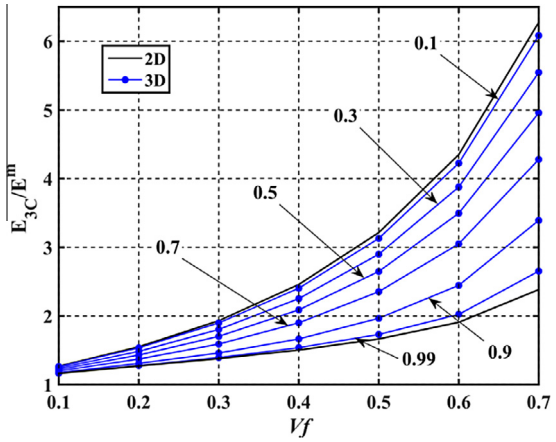

Fig. 7. Results for transverse Young modulus E_{3C} for 3D model and 2D model with values of damage parameter $pd = 1$ and Sq configuration.

For small values of *pd*, both configuration predict almost the same values; however, some differences are found for $pd = 1$ and for $0.4 \leqslant ld \leqslant 0.8$. For *ld* approaching 1, both damage cases yield similar E_{2T} values, which is consistent with the 3D model approaching the 2D model.

Regarding influence of the aspect ratio, β, results for E_{2T} are shown in Fig. 10 for composites having $1 \leqslant \beta \leqslant 100$, for $Vf = 70\%$,

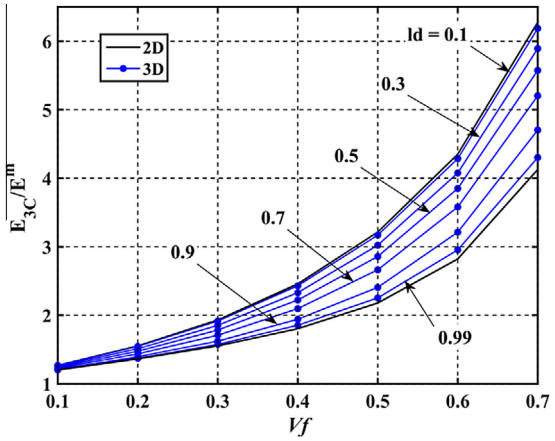

Fig. 8. Results for transverse Young modulus E_{3C} for 3D model and 2D model with values of damage parameter $pd = 0.5$ and Sq configuration.

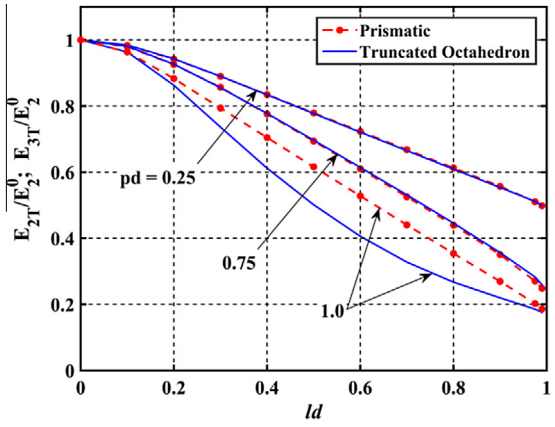

Fig. 9. Influence of damage distribution in the normalized transverse Young modulus with Hx fiber configuration and $Vf = 50\%$.

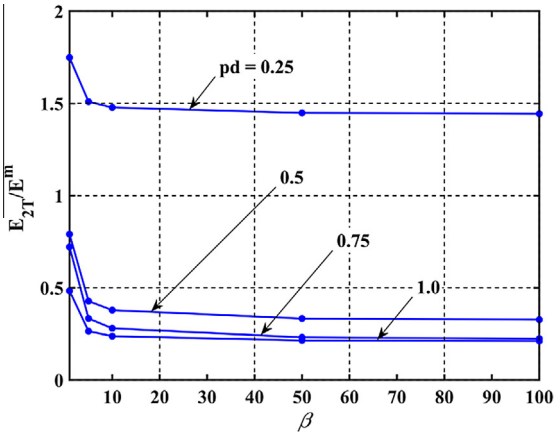

Fig. 10. Influence of aspect ratio β in the normalized transverse Young modulus with Sq fiber configuration, $Vf = 70\%$, and $ld = 0.99$.

Sq fiber configuration, $ld = 0.99$, and various values of pd. Results for each pd are almost constant with β, except for small values of $\beta < 5$.

The influence of fiber configuration (either Sq or Hx) with damage is shown in Fig. 11 for E_{2T} normalized with respect to $E_2^0 = 13.87$ GPa without damage for Hx; and $E_2^0 = 17.4$ GPa for Sq;

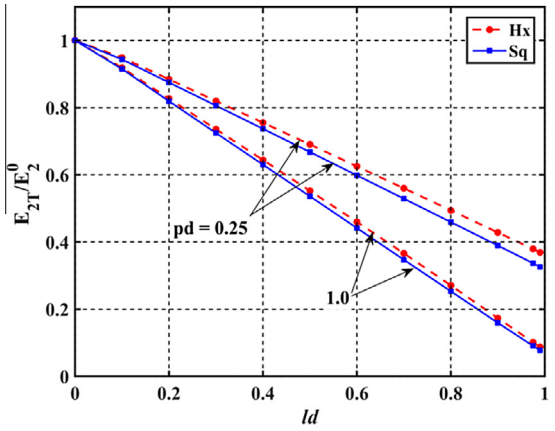

Fig. 11. Influence of fiber configuration in the normalized transverse Young modulus. Results for Sq and Hx fiber configuration, $Vf = 60\%$, and $\beta = 5$.

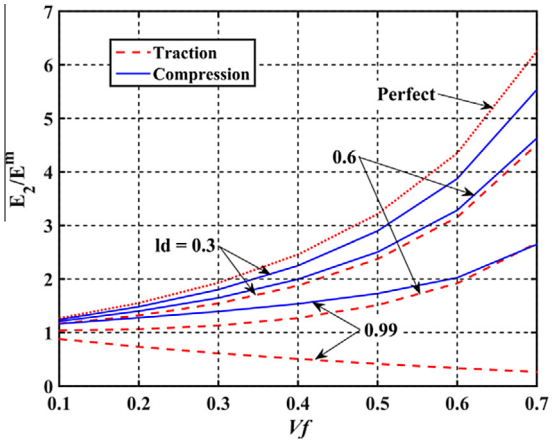

Fig. 12. Influence of fiber volume fraction in the normalized transverse Young modulus. Results for Sq fiber configuration, $pd = 1$, and $\beta = 5$.

values of $Vf = 60\%$ and $\beta = 5$ were considered. There is an almost linear reduction in modulus E_{2T} with ld. For the same damage condition, the Sq configuration is the most affected one.

The influence of Vf on the E_2 modulus has been studied for Sq configuration, $\beta = 5$, and $pd = 1$. Results are plotted in Fig. 12, in which tensile and compressive E_2 modulii are identified for $ld = 0.3$, 0.6, and 0.99, together with a configuration without damage. The tensile modulus shows higher changes than the compressive modulus; Teng [18] reported similar conclusions for models having damage parameters $ld = pd = 1$, so that the problem was classified as behaving like a bi-modular material (different modulus in tension and in compression). The transverse modulus presents reductions for all Vf considered, but effects are more severe for high Vf values; such trend has also been reported for shear modulus in axial direction in Ref. [12] for $ld = 1$.

4. Analytic forms of elastic constants in terms of damage parameters

The parametric studies reported in the last section illustrate the behavior of a damaged UC; however, the purpose of this study is not just to provide qualitative aspects of the response, but the results are next used to obtain modified elastic properties as used in CLT, to account for effects due to interface damage. To achieve this, the studies are approximated by analytical functions of elastic constants in terms of damage parameters.

Least Squares Methods have been used to build the analytical functions based on 3D modeling. The functions are limited to $Vf = 70\%$, square Sq configurations and damage parameters covering the full range $0 \leqslant ld \leqslant 1$ y $0 \leqslant pd \leqslant 1$. To perform the approximations, specific values of the constituent components were used as follows: $E_f = 80$ GPa, $\nu_f = 0.2$, $E_m = 4$ GPa y $\nu_m = 0.35$, with $Rf = 3.5 \times 10^{-6}$ m and $\beta = 5$. Plots of numerical and analytical results are shown in Figs. 13–18 for elastic modulii normalized with respect to the undamaged value. Because of space restrictions, not all plots of equations can be shown in this paper; however, the results are given in the form of analytical expression in Appendix A, and can be represented or employed from them.

The E_1 (along the fiber) modulus is not significantly affected by the damage parameters considered, leading to 57.23 GPa in compression and 57.19 GPa in tension for maximum damage as expressed by $pd = 1$ and $ld = 0.99$. This property could also be estimated by the rule of mixtures to obtain 57.2 GPa.

Modulus E_{3C} (under compression) showed the least reductions (see Fig. 13). E_{2C} has a similar trend, not shown here because of space restrictions. These properties show a slight nonlinearity with respect to *ld*. The E_{2T} modulus (Fig. 14) and E_{3T} have a more severe change under damage, and their change with *ld* is close to linear.

Regarding damage influence on G_{23}, G_{12}, and E_{2T}, there are significant reductions with *pd* for small *pd* values (i.e. $pd = 0.25$). For the same range in *pd*, modulii G_{13} and E_{3T} did not present a comparable change. This effect depends on the location of debonding and the direction of load and has been reported for $ld = 1$ in Ref. [11].

Poisson's ratio ν_{23C} refers to strains in direction 3 caused by a compression in direction 2; results for this Poisson value are given in Fig. 17: There is an increase with increasing damage levels. Because there is debonding at interface, the fiber cannot transfer tensile load to the matrix in zones in which the normal to the interface is almost parallel to the direction 3. The crack opens in these zones thus increasing the macroscopic strain in direction 3 with respect to the undamaged value.

The ν_{23T} Poisson coefficient has been studied with results shown in Fig. 18 as a function of *pd*. A tensile strain in direction 2 in this case increases the strain in this direction because the crack opens in zones close to the direction 2. However, for $pd = 1$ there is a small increase in ν_{23T} caused by an increase in macroscopic strain in direction 3 in comparison with the constraint given by the fiber for $pd = 0.75$.

Poisson ratios ν_{21C}, ν_{21T}, ν_{31C}, and ν_{31T} have similar trends as modulii E_{2C}, E_{2T}, E_{3C}, and E_{3T}, respectively. Reductions are computed respect to the undamaged case because the crack at the interface does not allow an effective force transfer in direction 1.

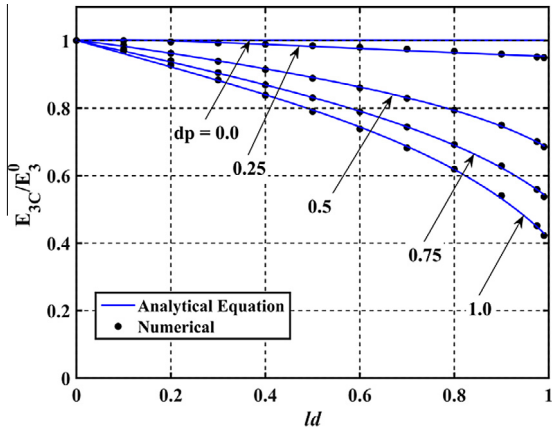

Fig. 13. Results for the normalized transverse Young modulus E_{3C}, from 3D model and analytic equation, as a function of *ld* and *pd* with Sq configuration, $Vf = 70\%$ and $\beta = 5$.

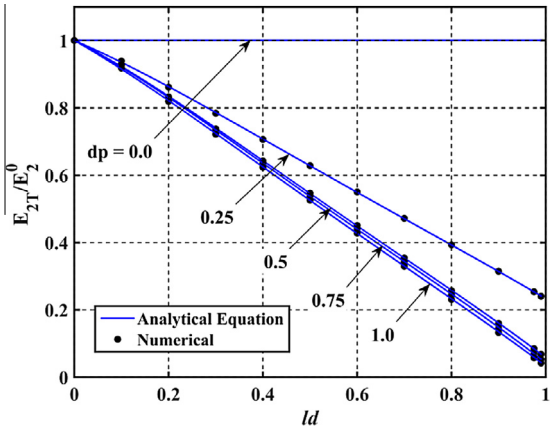

Fig. 14. Results for the normalized transverse Young modulus E_{2T}, from 3D model and analytic equation, as a function of *ld* and *pd* with Sq configuration, $Vf = 70\%$ and $\beta = 5$.

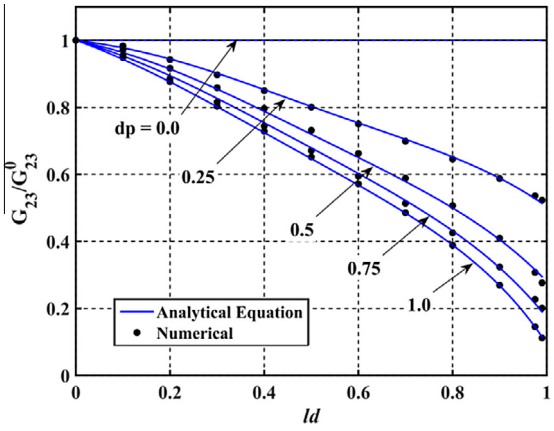

Fig. 15. Results for the normalized transverse shear modulus G_{23}, from 3D model and analytic equation, as a function of *ld* and *pd* with Sq configuration, $Vf = 70\%$ and $\beta = 5$.

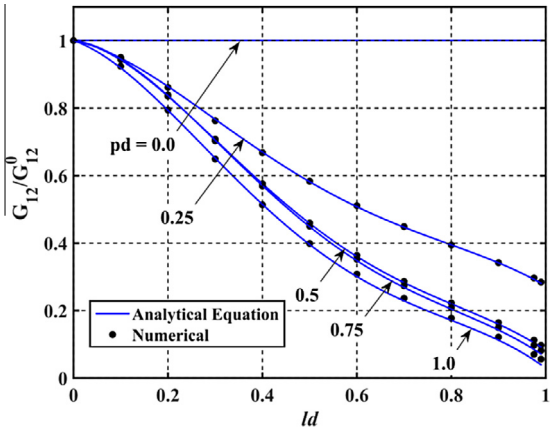

Fig. 16. Results for the normalized axial shear modulus G_{12}, from 3D model and analytic equation, as a function of *ld* and *pd* with Sq configuration, $Vf = 70\%$ and $\beta = 5$.

5. Application to Classical Lamination Theory

The explicit equations to obtain elastic properties at UC based on interface damage characteristics can next be used as a part of a macro-level analysis. This section reports an application to obtain

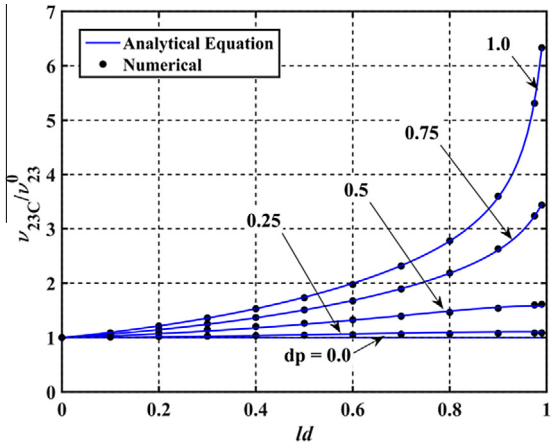

Fig. 17. Results for the normalized Poisson ratio ν_{23C}, from 3D model and analytic equation, as a function of *ld* and *pd* with Sq configuration, *Vf* = 70% and β = 5.

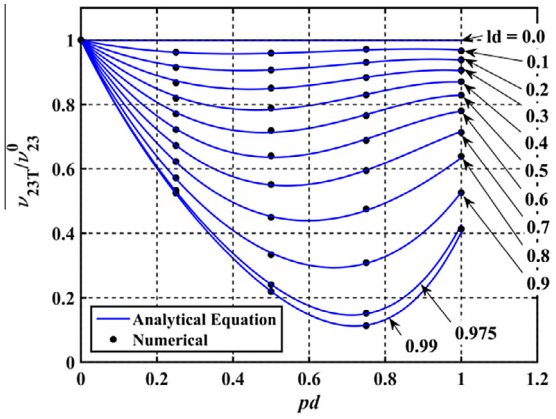

Fig. 18. Results for the normalized Poisson ratio ν_{23T}, from 3D model and analytic equation, as a function of *ld* and *pd* with Sq configuration, *Vf* = 70% and β = 5.

the maximum displacement in a laminated plate using CLT [1] in a Finite Element model; this allows performing a macro analysis in terms of micro and macro variables.

Consider a laminated [0/90] square plate having a bimodular material behavior (see Ref. [32]), with the origin of the (x, y) axis placed at a corner. Simply supported boundary conditions are given by

$$w = 0 \quad \text{in} \quad y = 0; \quad y = a; \quad x = 0; \quad \text{and} \quad x = a \tag{15}$$

$$v = 0 \quad \text{in} \quad x = 0 \quad \text{and} \quad x = a \tag{16}$$

$$u = 0 \quad \text{in} \quad y = 0 \quad \text{and} \quad y = a \tag{17}$$

The pressure q is given by

$$q = -1 \text{ kPa} \times \sin\left(\frac{\pi}{a}x\right) \sin\left(\frac{\pi}{a}y\right) \tag{18}$$

A Finite Element model was employed to solve this plate using ABAQUS, with a 16 × 16 mesh of linear shell elements (element S4R in the ABAQUS nomenclature). On account of the different material properties in tension and compression, the laminate in compression in direction 2 (0° orientation) has a modulus E_{2C}, whereas the laminate at 90° has a modulus E_{2T}. Because the present [0/90] laminate is under bending, an influence will be reflected in transverse elastic modulus rather than in shear modulus.

Table 1
Displacement at the center of the plate (normalized with respect to the undamaged value, w^0 = 2.11 mm), for different damaged regions and sizes for *ld* = *pd* = 1. Plate dimensions: side *a* = 2 m. Finite Element mesh has 16 × 16 elements.

Damaged lamina	Size of damaged region	Position of damaged region	
		Corner	Center
90°	$a/4 \times a/4$	1.107	1.205
90°	$a/2 \times a/2$	1.267	1.415
0° and 90°	$a/4 \times a/4$	1.130	1.292
0° and 90°	$a/2 \times a/2$	1.399	1.684

Table 2
Displacement at the center of the plate (normalized with respect to the undamaged value, w^0 = 2.11 mm), for different damaged regions and sizes for *ld* = 0.4 and *pd* = 0.7. Plate dimensions: side *a* = 2 m. Finite Element mesh has 16 × 16 elements.

Damaged lamina	Size of damaged region	Position of damaged region	
		Corner	Center
90°	$a/4 \times a/4$	1.080	1.093
90°	$a/2 \times a/2$	1.107	1.130
0° and 90°	$a/4 \times a/4$	1.090	1.089
0° and 90°	$a/2 \times a/2$	1.120	1.127

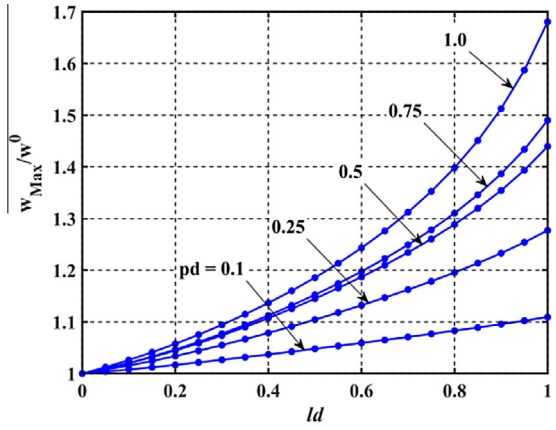

Fig. 19. Displacement at the center of the plate (normalized with respect to the undamaged value, w^0 = 2.11 mm), for different damaged parameters *ld* and *pd*. Plate dimensions: side *a* = 2 m; both lamina damaged. Finite Element mesh has 16 × 16 elements.

To investigate the behavior under damage, several macro scenarios were investigated. The plate was assumed to be damaged in a square region, which was placed at the center or at a corner of the plate. Damage was assumed to affect the top layer (90° lamina) or both, top and bottom layers. Material properties were evaluated using the formulation presented in this paper, for values of damage parameters *ld* = 0.4, *pd* = 0.7 and *ld* = *pd* = 1. Results are presented in Tables 1 and 2 in terms of displacement at the center of the plate. As expected, the most severe increase in displacements occurs with damage affecting the central region, with damage in all layers and for the values *ld* = *pd* = 1, with an increase of 68% with respect to the undamaged configuration.

A second investigation included the influence of damage parameters *ld* and *pd* on the response, for a plate having a central damage zone of dimensions $a/2 \times a/2$ in both layers. Results are plotted in Fig. 19, and show a nonlinear response with an increase in damage parameters.

6. Conclusions

Computational micro-mechanics has been used in this work to evaluate changes in elastic properties of GFRP composites with fiber-matrix localized detachment. It is assumed that damage causes a crack-like behavior at the interface with the possibility of contact due to deformations of the matrix. Contact without friction has been introduced in the model.

Different damage scenarios have been taken into account by changing the zone affected by damage in the direction of the fiber (*ld*) and on the perimeter of the fiber (*pd*) in the cross section. Space distributions are also considered in 3D modeling, thus affecting the zone of damage with respect to neighboring fibers. The end-product of the study is a set of analytical expressions for elastic parameters in terms of damage parameters.

The elastic modulus in the fiber direction is not sensitive to this form of damage because this behavior is controlled by the fiber; this conclusion had previously been drawn from experiments in Ref. [3]. But there is a severe consequence of damage on the other properties with increasing damage values; this is consistent with numerical results presented in Refs. [14,18]. The present studies are capable of capturing a bi-modular behavior in the transverse direction. Transverse moduli under tension have an almost linear reduction with respect to *ld*, whereas shear and compression transverse modulii show a nonlinear relation with damage parameters.

The present results have been presented in such a way that they can be used as off-line, pre-defined lamina properties with damage in coupling micro and macro scales, without the need to perform in-time micro scale computations. This coupling may be performed using either Classical Lamination Theory, or else in Finite Element computations at macro level.

Acknowledgments

NDB and LAG were supported by CONICET, the Science Research Council of Argentina during this research. The authors thank the support received from grants of CONICET (PIP 0126), SECyT-UNC and UTN-FRC (UTI 2119).

Appendix A

The analytical expressions of elastic properties, as they are used in CLT at the macro scale, have been obtained for damage parameters *ld* and *pd*. To simplify the expressions the nomenclature $x = ld$, and $y = pd$ is used in this Appendix. Due to their simplicity, polynomials have been used to derive Eqs. (21)–(33), and their final form was obtained by trial and error as explained in below.

For each property considered, the procedure begins with a trial polynomial in the form

$$p(x,y) = \sum_{i=0}^{N} c_i x^i y^i \tag{19}$$

The c_i coefficients are next evaluated by means of LSM and the relative error is evaluated for each property at the macro level as obtained by the Finite Element method p_{FEM}

$$e(x,y) = \frac{abs(p(x,y) - p_{FEM}(x,y))}{\max(p_{FEM})} 100\% \tag{20}$$

where $\max(p_{FEM})$ is the maximum value for the elastic property obtained from the Finite Element model. If the relative difference is higher than 2%, then the value of N is increased until an acceptable error is reached. For the reverse procedure of reducing the number of terms, a term is eliminated in the polynomial and the error in the new equation is studied next.

In cases in which there are oscillations in the results of polynomials, an alternative form is considered as a division between two polynomials. A second order polynomial is first considered and the coefficients are evaluated; if the error is higher than 2% then a new term is added to both dividend and divisor. Thus, all equations presented in this work have an error defined by Eq. (20) and less than 2%.

Values of the coefficients are given in Tables A1 and A2. Notice that coefficients take a different value in each equation. Shear and transverse modulii are expressed in GPa units.

$$\begin{aligned} \nu_{23T} = {} & a0 + a1xy + a2xy^2 + a3xy^3 + a4x^2y^2 + a5x^2y^3 \\ & + a6x^2y^4 + a7x^3y^2 + a8x^3y^3 + a9x^4y^3 + a10x^4y^4 \end{aligned} \tag{21}$$

$$\begin{aligned} \nu_{23C} = {} & a0 + \frac{(a1 + a2xy + a3x^2y + a4y + a5x)xy}{b0 + a9xy + a10y + a11y^2 + a12y^3} \\ & \text{with } b0 = a6 + a7x^2 + a8x^3 \end{aligned} \tag{22}$$

$$\begin{aligned} \nu_{21T} = {} & a0 + a1xy + a2xy^2 + a3xy^4 + a4xy^5 + a5x^2y + a6x^3y \\ & + a7x^3y^6 + a8x^4y + a9x^4y^7 + a10x^5y^8 + a11x^7y^7 \\ & + a12x^7y^8 \end{aligned} \tag{23}$$

$$\nu_{21C} = a0 + a1xy^2 + a2xy^3 + a3xy^4 + a4x^4y^3 \tag{24}$$

$$\nu_{31T} = a0 + \frac{(a1 + a2x + a3y^2 + a4x^2)xy}{a5 + a6x + a7x^2 + a8x^3 + a9y + a10y^2} \tag{25}$$

Table A1
Coefficients of equations for elastic shear modulii and Poisson's ratios.

	ν_{23T}	ν_{23C}	ν_{21T}	ν_{21C}	ν_{31T}	ν_{31C}	G_{12}	G_{13}	G_{23}
*a*0	0.2188	0.2187	0.102	0.102	0.102	0.102	7.984	7.996	5.442
*a*1	−0.5318	12.46	−0.3912	−0.2327	−0.00293	−0.00191	−18.67	−1.568	−14.29
*a*2	1.0515	−1.288	0.6027	0.4535	−0.0099	−0.0252	45.37	1.559	0.522
*a*3	−0.5952	59.53	−0.5756	−0.2587	−0.0826	0.01727	−30.55	0.5858	−9.801
*a*4	−1.6723	−67.02	0.2891	−0.023	0.0107	0.5762	−110.9	−3.691	−3.254
*a*5	2.643	−16.26	−0.1572	–	0.9542	−0.1516	101.6	−40.53	9.834
*a*6	−0.985	−114.1	0.1982	–	−0.0641	0.5885	−22.1	2.556	2.915
*a*7	1.1808	41.07	0.2894	–	0.0482	−0.4068	177.8	0.4392	−8.064
*a*8	−1.1436	−34.57	−0.0898	–	−0.0565	0.01988	−183.4	−0.2514	12.41
*a*9	−1.5203	278.9	−0.6349	–	−2.478	−2.22	41.5	−7.471	−5.749
*a*10	1.4287	−84.37	0.4429	–	2.465	3.399	15.81	6.243	2.27
*a*11	–	−80.33	0.1729	–	–	−1.648	−85.4	4.389	1.138
*a*12	–	−15.56	−0.244	–	–	–	105	–	−1.475
*a*13	–	–	–	–	–	–	−43.81	–	–

Table A2
Coefficients for transverse elastic modulii.

	E_{2T}	E_{2C}	E_{3T}	E_{3C}
$a0$	25.02	25.02	25.11	25.12
$a1$	−106.5	−64.92	−2579	5.56
$a2$	236.2	133.2	1098	−34.17
$a3$	−224.3	−77.88	−218.2	21.02
$a4$	74.63	−4.881	−2.59E4	−73.41
$a5$	−66.49	–	−1784	16.2
$a6$	51	–	1560	4.426
$a7$	73.32	–	−225.2	2.87
$a8$	−30.91	–	279.5	−2.246
$a9$	−22.04	–	−122.5	−18.14
$a10$	−28.1	–	−4667	20.5
$a11$	19	–	4349	−2.996
$a12$	–	–	34.77	–

$$v_{31C} = a0 + \frac{(a1 + a2xy + a3y^2x)xy}{b1 + a7x^3 + a8xy^2 + a9y + a10y^2 + a11y^3} \quad \text{with } b1 = a4 + a5x + a6x^2 \tag{26}$$

$$G_{12} = a0 + a1xy + a2xy^2 + a3xy^3 + a4x^2y + a5x^2y^2 + a6x^2y^3 + a7x^3y + a8x^3y^2 + a9x^3y^3 + a10x^3y^4 + a11x^4y + a12x^4y^2 + a13x^4y^3 \tag{27}$$

$$G_{13} = a0 + \frac{(a1 + a2x + a3x^2 + a4y^3 + a5xy^3)xy}{a6 + a7x + a8x^2 + a9y + a10y^2 + a11y^4x^2} \tag{28}$$

$$G_{23} = a0 + \frac{(a1 + a2x + a3x^2 + a4y^3 + a5x^2y^2)xy}{b2 + a9x^3 + a10y + a11y^2 + a12y^3x^3} \quad \text{with } b2 = a6 + a7x + a8x^2 \tag{29}$$

$$E_{2T} = a0 + a1xy + a2xy^2 + a3xy^3 + a4xy^4 + a5x^2y + a6x^2y^2 + a7x^3y + a8x^3y^2 + a9x^3y^3 + a10x^4y + a11x^4y^3 \tag{30}$$

$$E_{2C} = a0 + a1xy^2 + a2xy^3 + a3xy^4 + a4x^4y^3 \tag{31}$$

$$E_{3T} = a0 + \frac{(a1 + a2x + a3x^2 + a4y^3 + a5x^2y^2)xy}{b3 + a9x^3 + a10y + a11y^2 + a12y^3x^3} \quad \text{with } b3 = a6 + a7x + a8x^2 \tag{32}$$

$$E_{3C} = a0 + \frac{(a1 + a2x + a3x^2 + a4y^3 + a5xy^3)xy}{a6 + a7x + a8x^2 + a9y + a10y^2 + a11y^4x^2} \tag{33}$$

References

[1] Barbero EJ. Introduction to composite materials design. Boca Raton: CRC Press; 2010.
[2] Reddy JN. A simple higher-order theory for laminated composite plates. J Appl Mech 1984;51(4):745–52.
[3] Kajorncheappunngam S, Gupta RK, GangaRao HV. Effect of aging environment on degradation of glass-reinforced epoxy. ASCE J Compos Constr 2002;6(1):61–9.
[4] Faguaga E, Pérez CJ, Villarreal N, Rodriguez ES, Alvarez V. Effect of water absorption on the dynamic mechanical properties of composites used for windmill blades. Mater Des 2012;36:609–16.
[5] De La Osa O, Alvarez VA, Fraga AN, Mammone EM, Vázquez A. Loss of mechanical properties by water absorption of vinyl-ester reinforced with glass fiber. J Reinf Plast Compos 2006;25(2):215–21.
[6] Kotani M, Yamamoto Y, Shibata Y, Kawada H. Strength prediction method for unidirectional GFRP after hydrothermal aging. Adv Compos Mater 2011;20(6):519–35.
[7] Ayadi A, Nouri H, Guessasma S, Roger F. Determination of orthotropic properties of glass fibre reinforced thermoplastics using X-ray tomography and multiscale finite element computation. Compos Struct 2016;136:635–49.
[8] Naouar N, Vidal-Salle E, Schneider J, Maire E, Boisse P. 3D composite reinforcement meso FE analyses based on X-ray computed tomography. Compos Struct 2015;132:1094–104.
[9] Kamiński MM. Computational mechanics of composite materials. London UK: Springer; 2005.
[10] Godoy LA, Mondragón V, Pando M, Acosta FJ. Stress redistributions in unit cells of fibre-reinforced polymer composites with interface degradation. Int J Microstruct Mater Prop 2013;8(3):185–206.
[11] Teng H. On stiffness reduction of a fiber-reinforced composite containing interfacial cracks under longitudinal shear. Mech Mater 1992;13(2):175–83.
[12] Teng H. Effective longitudinal shear modulus of a unidirectional fiber composite containing interfacial cracks. Int J Solids Struct 1992;29(12):1581–95.
[13] Kim SY, Moon HJ, Earmme YY. Effective elastic moduli in fiber reinforced composite with circular-arc shaped interfacial cracks. Int J Fract 1995;71(1):85–93.
[14] Kushch VI, Shmegera SV, Mishnaevsky L. Elastic interaction of partially debonded circular inclusions. II. Application to fibrous composite. Int J Solids Struct 2011;48(16):2413–21.
[15] Kushch VI, Shmegera SV, Mishnaevsky L. Elastic interaction of partially debonded circular inclusions. I. Theoretical solution. Int J Solids Struct 2010;47(14):1961–71.
[16] Takahashi K, Chou TW. Transverse elastic moduli of unidirectional fiber composites with interfacial debonding. Metall Trans A 1988;19(1):129–35.
[17] Shan HZ, Chou TW. Transverse elastic moduli of unidirectional fiber composites with fiber/matrix interfacial debonding. Compos Sci Technol 1995;53(4):383–91.
[18] Teng H. Transverse stiffness properties of unidirectional fiber composites containing debonded fibers. Compos A Appl Sci Manuf 2007;38(3):682–90.
[19] Rodriguez-Ramos R, de Medeiros R, Guinovart-Diaz R, Bravo-Castillero J, Otero JA, Tita V. Different approaches for calculating the effective elastic properties in composite materials under imperfect contact adherence. Compos Struct 2013;99:264–75.
[20] Guinovart-Díaz R, Rodríguez-Ramos R, Bravo-Castillero J, López-Realpozo JC, Sabina FJ, Sevostianov I. Effective elastic properties of a periodic fiber reinforced composite with parallelogram-like arrangement of fibers and imperfect contact between matrix and fibers. Int J Solids Struct 2013;50(13):2022–32.
[21] Sabina FJ, Guinovart-Díaz R, Rodriguez-Ramos R, López-Realpozo JC, Bravo-Castillero J. Overall properties in fibrous elastic composite with imperfect contact condition. Int J Eng Sci 2012;61:142–55.
[22] Nemat-Nasser S, Hori M. Micromechanics: overall properties of heterogeneous materials. Amsterdam: North-Holland; 1999.
[23] Zohdi TI, Wriggers P. An introduction to computational micromechanics. Berlin Germany: Springer; 2008.
[24] Mões N, Dolbow J, Belytschko T. A finite element method for crack growth without remeshing. Int J Numer Meth Eng 1999;46(1):131–50.
[25] Guo Z, Shi X, Chen Y, Chen H, Peng X, Harrison P. Mechanical modeling of incompressible particle-reinforced neo-Hookean composites based on numerical homogenization. Mech Mater 2014;70:1–17.
[26] Abadi MT. Characterization of heterogeneous materials under shear loading at finite strain. Compos Struct 2010;92(2):578–84.
[27] Zahr-Viñuela J, Pérez-Castellanos J. Elastic constants and isotropy considerations for particulate metal-matrix composites. A multi-particle, cell-based approach. Compos A Appl Sci Manuf 2011;42(5):521–33.
[28] Abaqus v. 6.7. Dassault Systèmes, Providence, RI, USA; 2009.
[29] Oller S, Miquel Canet J, Zalamea F. Composite material behavior using a homogenization double scale method. ASCE J Eng Mech 2005;131(1):65–79.
[30] Kamiński M. Sensitivity and randomness in homogenization of periodic fiber-reinforced composites via the response function method. Int J Solids Struct 2009;46(3):923–37.
[31] Seber GAF, Wild CJ. Nonlinear regression. Hoboken: John Wiley & Sons, Inc.; 2003.
[32] Reddy JN, Chao WC. Finite-element analysis of laminated bimodulus composite-material plates. Comput Struct 1980;12(2):245–51.